Electronic Supplementary Material (ESI) for Journal of Materials Chemistry A.

SUPPORTING INFORMATION

Thickness Dependent OER Electrocatalysis of Epitaxial $LaFeO_3$ Thin Films

Andricus R. Burton[a†], Rajendra Paudel[b†], Bethany Matthews[c], Michel Sassi[d], Steven R. Spurgeon[c], Byron H. Farnum[a*], Ryan B. Comes[b*]

[a]Department of Chemistry and Biochemistry, Auburn University, Auburn, AL 36849
[b]Department of Physics, Auburn University, Auburn, AL 36849
[c]Energy and Environment Directorate, Pacific Northwest National Laboratory, Richland, WA 99352
[d]Physical and Computational Sciences Directorate, Pacific Northwest National Laboratory, Richland, WA 99352

*corresponding authors: farnum@auburn.edu, ryan.comes@auburn.edu
†equal contribution

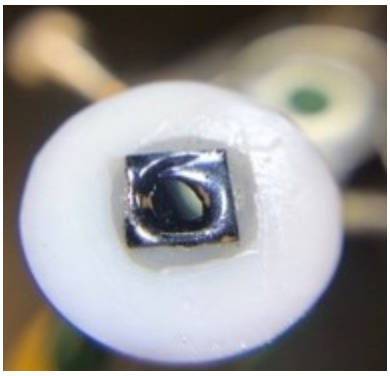

Figure S1. Fabricated n-STO/LFO on top of a GC rotating disk electrode. GC disk is completely covered by 5 mm x 5 mm n-STO substrate. Larger white area is a Teflon shaft.

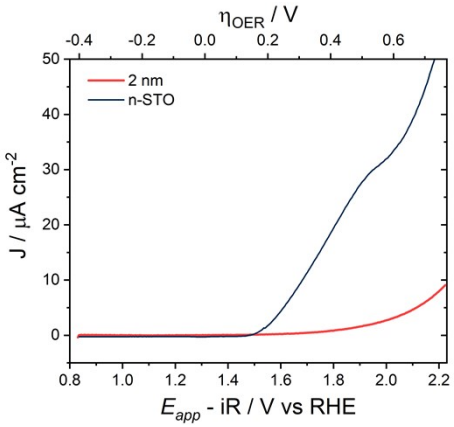

Figure S2. Anodic scan of CV data collected for a bare (001) n-STO electrode. Data collected in O2 saturated 0.1 M KOH aqueous electrolyte at 20 mV s^{-1} scan rate and 2000 rpm rotation.

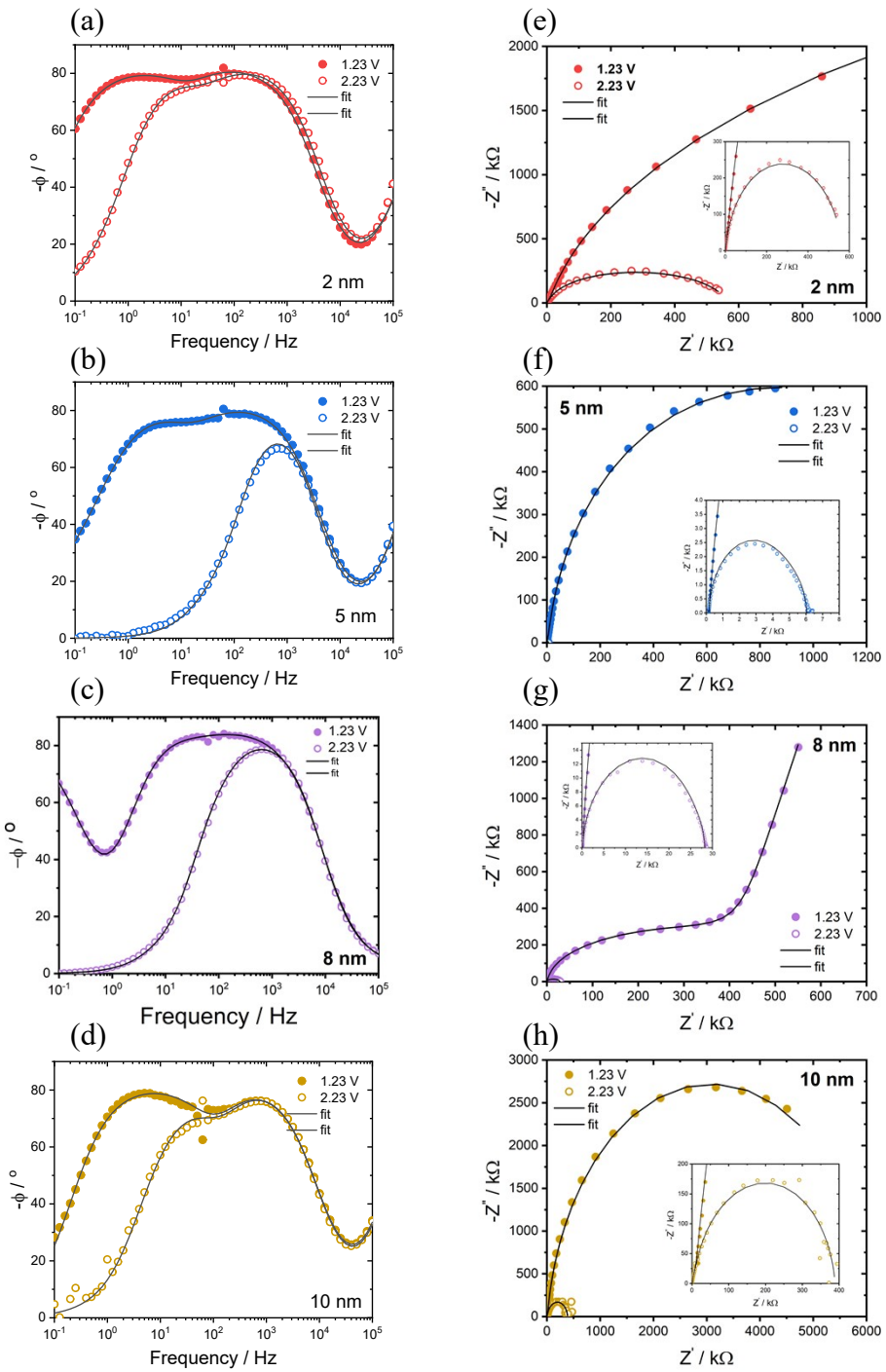

Figure S3. Bode-phase (a-d) and Nyquist (e-h) plots for 2, 5, 8, and 10 nm LFO films obtained from EIS experiments performed at 1.23 and 2.23 V. Overlaid fits were derived from the equivalent circuit model shown in **Figure 6e** of the main text.

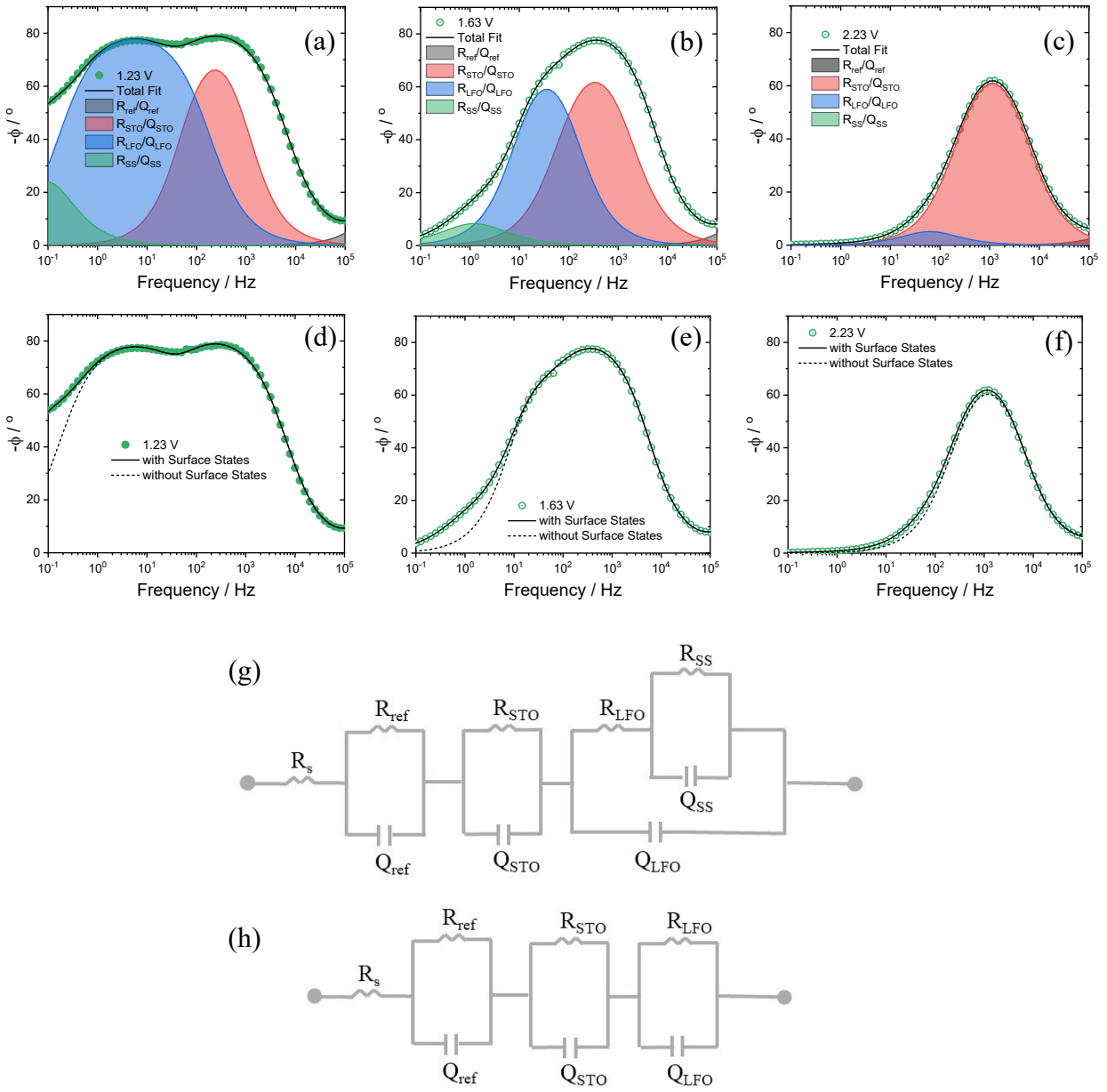

Figure S4. Bode-phase plots for 6 nm LFO at 1.23, 1.63, and 2.23 V. Solid lines show the full simulation according to the circuit model shown in part (g). (a-c) Individual colored peaks represent contributions from different parallel R/Q circuit elements. Grey – R_{ref}/Q_{ref}, Red – R_{STO}/Q_{STO}, Blue – R_{LFO}/Q_{LFO}, Green – R_{SS}/Q_{SS}. Note that the total fit is not to be viewed as a linear summation of individual peaks. R_{STO}/Q_{STO} was mostly unchanged as a function of applied potential while R_{LFO}/Q_{LFO} and R_{SS}/Q_{SS} decreased in magnitude as the potential was shifted positive. (d-f) Comparison of fitting data for two circuit models. The solid lines are the same as that in (a-c) and include surface states as shown in part (g) which includes the nested surface state elements R_{SS} and Q_{SS}. The dashed lines represent simulations with the circuit model shown in part (h) which excluded surface states and uses the same circuit parameter values for R_{ref}, Q_{ref}, R_{STO}, Q_{STO}, R_{LFO}, and Q_{LFO}. R_s = 1 Ω in all cases.

Table S1. Summary of EIS Fitting Parameters for E_{app} = 1.23 V vs RHE

	2 nm	5 nm	6 nm	8 nm	10 nm
Q_{ref}	17 ± 82 nF $s^{\alpha-1}$	6.8 ± 10. nF $s^{\alpha-1}$	0.7 ± 3.2 nF $s^{\alpha-1}$	0.1 ± 6.6 nF $s^{\alpha-1}$	2.0 ± 5.4 nF $s^{\alpha-1}$
α_{ref}	0.92 ± 0.36	1.0 ± 0.1	1.0 ± 0.1	1.0 ± 1.8	1.0 ± 0.05
R_{ref}	190 ± 23 Ω	160 ± 21 Ω	191 ± 26 Ω	150 ± 24 Ω	410 ± 61
Q_{STO}	2.0 ± 1.9 µF $s^{\alpha-1}$	2.2 ± 1.8 µF $s^{\alpha-1}$	0.78 ± 0.73 µF $s^{\alpha-1}$	2.8 ± 3.6 µF $s^{\alpha-1}$	0.17 ± 0.15 µF $s^{\alpha-1}$
α_{STO}	0.99 ± 0.15	0.93 ± 0.11	1.0 ± 0.1	0.82 ± 0.10	0.98 ± 0.10
R_{STO}	5.1 ± 0.0 kΩ	5.4 ± 0.0 kΩ	4.1 ± 0.0 kΩ	5.0 ± 0.0 kΩ	7.9 ± 0.0 kΩ
Q_{LFO}	0.56 ± 0.07 µF $s^{\alpha-1}$	0.62 ± 0.09 µF $s^{\alpha-1}$	0.36 ± 0.04 µF	0.17 ± 0.03 µF $s^{\alpha-1}$	0.13 ± 0.02 µF $s^{\alpha-1}$
α_{LFO}	0.92 ± 0.02	0.93 ± 0.03	0.91 ± 0.02	0.99 ± 0.03	0.92 ± 0.04
R_{LFO}	5.8 ± 0.0 MΩ	1.0 ± 0.0 MΩ	2.7 ± 0.0 MΩ	0.55 ± 0.0 MΩ	5.5 ± 0.0 MΩ
Q_{SS}	2.1 ± 9.7 µF $s^{\alpha-1}$	2.4 ± 2.3 µF $s^{\alpha-1}$	0.58 ± 0.42 µF	1.1 ± 0.2 µF $s^{\alpha-1}$	0.032 ± 1.4 µF $s^{\alpha-1}$
α_{SS}	0.5 ± 4.0	0.64 ± 0.71	0.91 ± 0.44	0.94 ± 0.09	1.0 ± 8.6
R_{SS}	21 ± 0.0 MΩ	1.0 ± 0.0 MΩ	4.6 ± 0.0 MΩ	71 ± 0.0 MΩ	0.69 ± 0.0 MΩ

R_s was set to 1 Ω for all fits; α is unitless; error expressed as standard error from the fitting analysis; an error of 0.0 indicates that the error was smaller than the significant figures of the mean value

Table S2. Summary of EIS Fitting Parameters for E_{app} = 2.23 V vs RHE

	2 nm	5 nm	6 nm	8 nm	10 nm
Q_{ref}	19 ± 114 nF $s^{\alpha-1}$	13 ± 31 nF $s^{\alpha-1}$	1.0 ± 14.1 nF $s^{\alpha-1}$	4.8 ± 367.2 nF $s^{\alpha-1}$	1.9 ± 5.3 nF $s^{\alpha-1}$
α_{ref}	0.91 ± 0.45	0.95 ± 0.18	0.91 ± 0.80	0.80 ± 5.47	1.0 ± 0.0
R_{ref}	190 ± 29 Ω	170 ± 23 Ω	210 ± 33 Ω	150 ± 35 Ω	420 ± 63 Ω
Q_{STO}	1.6 ± 1.4 µF $s^{\alpha-1}$	0.31 ± 0.18 µF $s^{\alpha-1}$	0.25 ± 0.15 µF $s^{\alpha-1}$	0.78 ± 1.5 µF $s^{\alpha-1}$	0.16 ± 0.17 µF $s^{\alpha-1}$
α_{STO}	0.92 ± 0.10	0.98 ± 0.06	0.94 ± 0.06	0.92 ± 0.18	1.0 ± 0.1
R_{STO}	5.5 ± 0.0 kΩ	4.8 ± 0.0 kΩ	4.1 ± 0.2 kΩ	4.2 ± 0.6 kΩ	5.9 ± 0.0 kΩ
Q_{LFO}	0.41 ± 0.08 µF $s^{\alpha-1}$	5.5 ± 37.4 µF $s^{\alpha-1}$	5.6 ± 17.7 µF	0.19 ± 0.13 µF $s^{\alpha-1}$	0.12 ± 0.34 µF
α_{LFO}	0.95 ± 0.04	1.0 ± 1.3	0.87 ± 0.56	1.0 ± 0.1	0.93 ± 0.05
R_{LFO}	4.9 ± 0.0 kΩ	0.96 ± 0.13 kΩ	1.0 ± 0.4 kΩ	23 ± 0.6 kΩ	360 ± 0.0 kΩ
Q_{SS}	5.8 ± 16.2 µF $s^{\alpha-1}$	49 ± 7,922 µF $s^{\alpha-1}$	4,600 ± 29,400 µF	18 ± 44 µF $s^{\alpha-1}$	1.1 ± 14.3 µF
α_{SS}	0.87 ± 1.27	1.0 ± 25.4	0.64 ± 1.3	1.0 ± 0.5	1.0 ± 3.8
R_{SS}	66 ± 0.0 kΩ	0.07 ± 0.13 kΩ	0.09 ± 0.37 kΩ	1.3 ± 0.6 kΩ	20. ± 1.8 kΩ

R_s was set to 1 Ω for all fits; α is unitless; error expressed as standard error from the fitting analysis; an error of 0.0 indicates that the error was smaller than the significant figures of the mean value

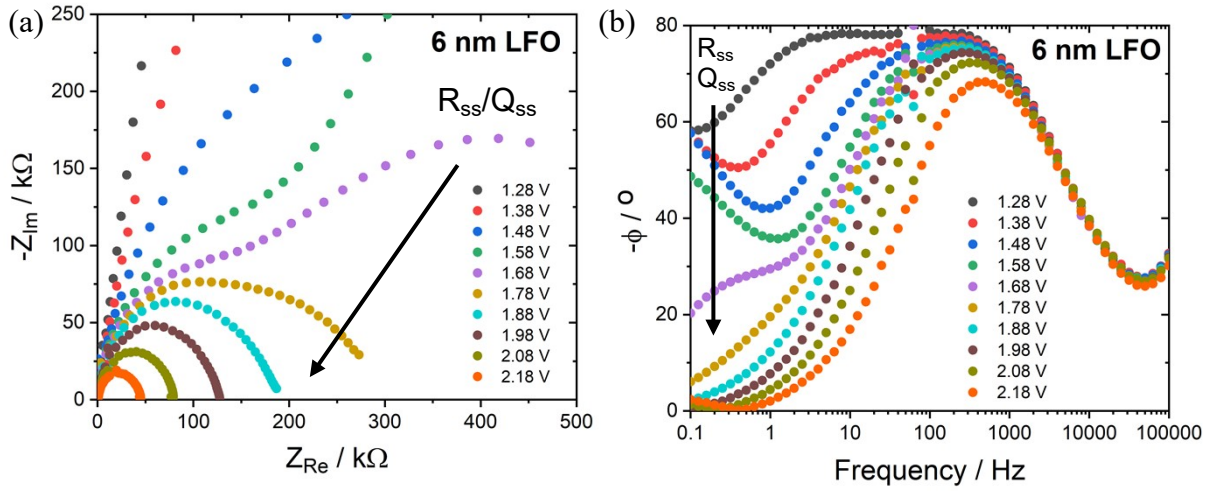

Figure S5. (a) Nyquist and (b) Bode-phase plots collected for a 6 nm LFO film with selected E_{app} values. The full range of E_{app} was from 1.23 to 2.23 V vs RHE with 50 mV steps.

Table S3. Summary of surface state EIS fitting parameters obtained from 6 nm LFO

E_{app}	Q_{ss} / F $s^{\alpha-1}$	α	R_{ss} / Ω	C_{ss} / F
1.23	1.9×10^{-7}	0.96	200,000,000	2.2×10^{-7}
1.28	2.3×10^{-7}	0.92	19,000,000	2.7×10^{-7}
1.33	3.7×10^{-7}	0.94	37,000,000	4.3×10^{-7}
1.38	5.0×10^{-7}	0.91	400,000,000	8.3×10^{-7}
1.43	6.7×10^{-7}	0.87	11,000,000	8.9×10^{-7}
1.48	1.0×10^{-6}	0.84	15,000,000	1.7×10^{-6}
1.53	1.4×10^{-6}	0.84	4,000,000	1.9×10^{-6}
1.58	1.7×10^{-6}	0.80	2,100,000	2.4×10^{-6}
1.63	2.2×10^{-6}	0.81	1,200,000	2.8×10^{-6}
1.68	2.3×10^{-6}	0.78	410,000	2.2×10^{-6}
1.73	2.2×10^{-6}	0.72	220,000	1.7×10^{-6}
1.78	2.0×10^{-6}	0.93	94,000	1.8×10^{-6}
1.83	1.9×10^{-6}	0.97	38,000	1.7×10^{-6}
1.88	1.0×10^{-6}	1.00	33,000	1.0×10^{-6}
1.93	5.0×10^{-7}	0.54	26,000	1.3×10^{-8}
1.98	5.9×10^{-9}	1.00	50,000	5.9×10^{-9}
2.03	1.0×10^{-11}	0.60	1,700	2.6×10^{-17}
2.08	1.0×10^{-11}	0.56	1,200	4.9×10^{-18}
2.13	1.0×10^{-11}	0.50	900	9.0×10^{-20}
2.18	8.1×10^{-8}	1.00	2,200	8.1×10^{-8}
2.23	1.0×10^{-11}	0.69	1,900	2.8×10^{-15}

$C_{ss} = (Q_{ss}^{1/\alpha})(R_{ss}^{1/\alpha-1})$

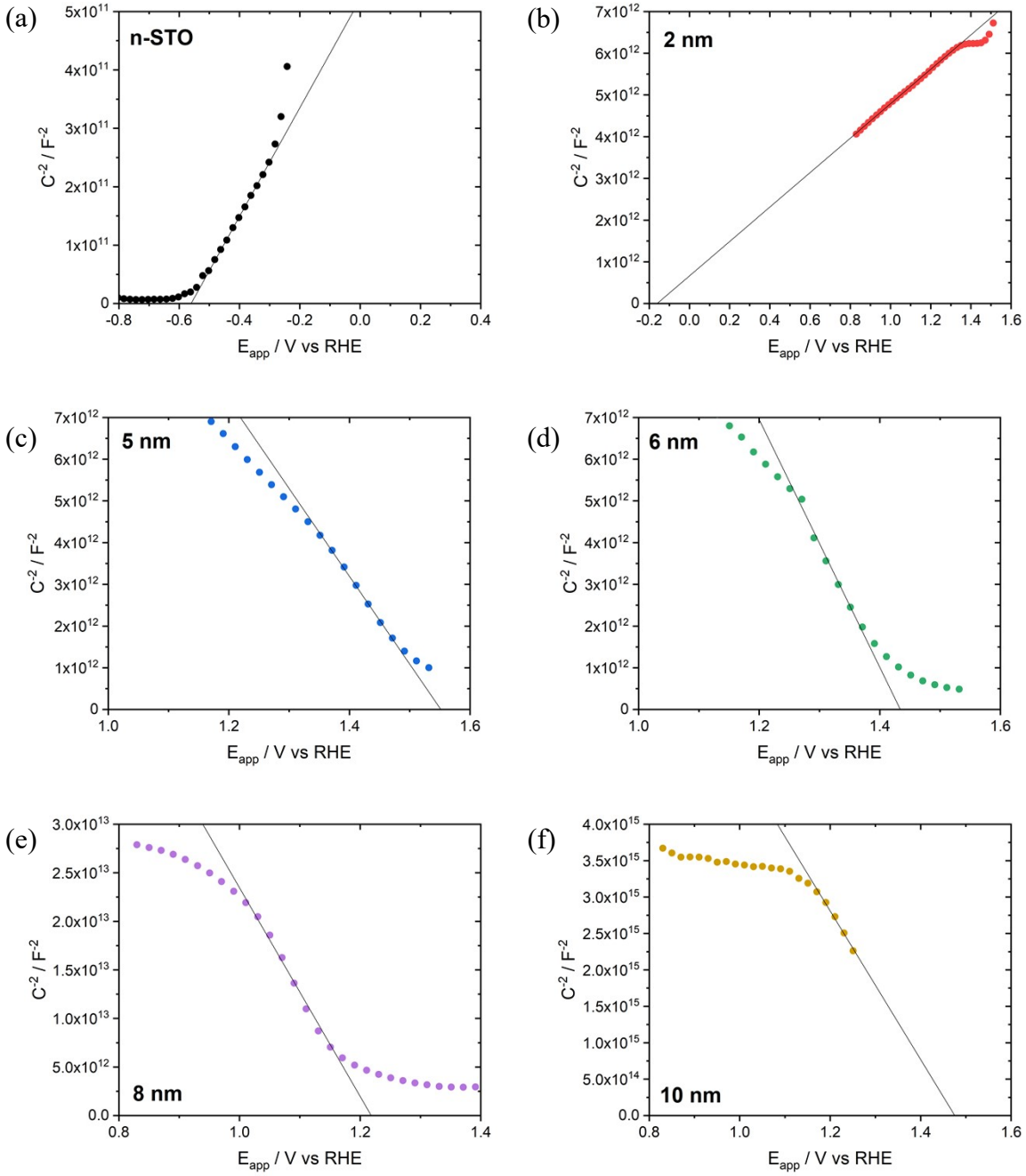

Figure S6. Mott-Schottky plots obtained at 0.5 Hz for (a-f) 0 (n-STO), 2, 5, 6, 8, and 10 nm LFO films.

Table S4. Summary of Mott-Schottky data

LFO / nm	E_{fb} / V vs RHE[a]	VBO / eV[b]
2	-0.19	0.61
5	1.52	2.32
6	1.40	2.20
8	1.19	1.99
10	1.43	2.23

[a]E_{fb} calculated from the Mott-Schottky equation; [b]VBO = E_{fb} – E_{vb}(LFO) + E_g(STO); E_{vb} (LFO) = 2.4 V vs RHE; E_g(STO) = 3.2 eV

Mott-Schottky Equation

$$\frac{1}{C^2} = \frac{2}{\varepsilon\varepsilon_o A^2 q N_A}\left(E_{app} - E_{fb} - k_B T/q\right)$$

C = interfacial capacitance (F)
ε = relative permittivity
ε_o = vacuum permittivity (8.85 x 10^{-12} F m^{-1})
A = electrode surface area (cm^2)
Q = fundamental charge (1.602 x 10^{-19} C)
N_A = density of acceptors (cm^{-3})
E_{app} = applied potential (V vs RHE)
E_{fb} = flat band potential (V vs RHE)
k_B = Boltzmann constant (1.38 x 10^{-23} J K^{-1})
T = temperature (298 K)

Based on the Mott-Schottky equation, E_{fb} was estimated by subtracting k_BT/q (= 0.0256 V) from the x-intercept of the Mott-Schottky plots.

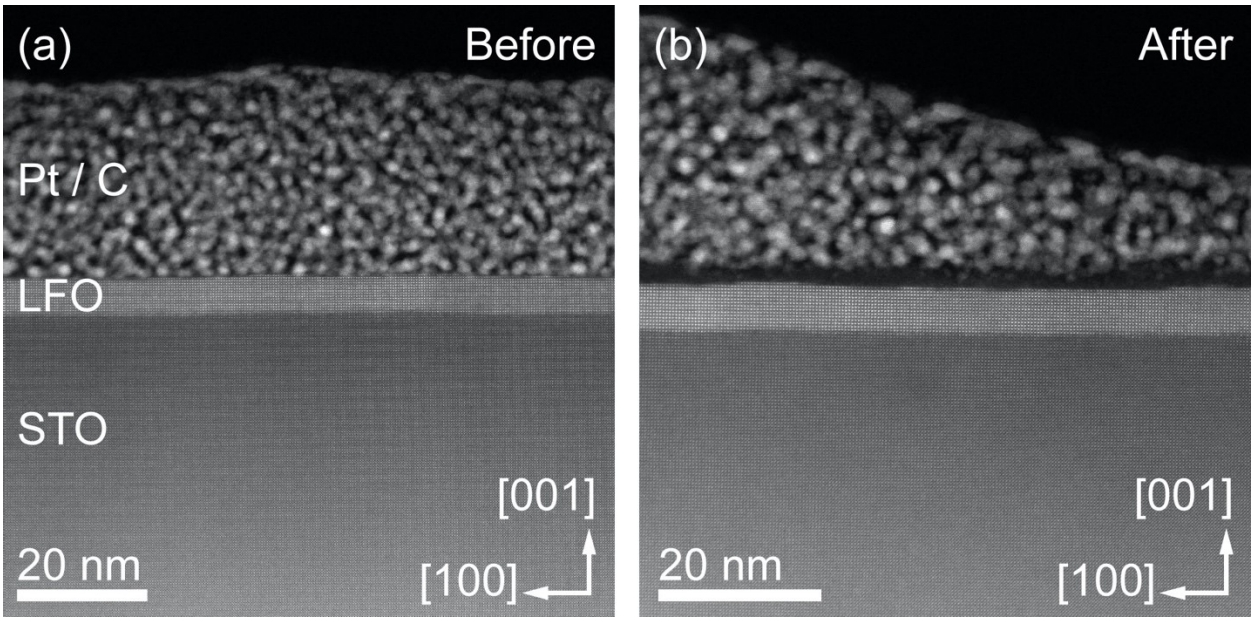

Figure S7. (a-b) Comparison of cross-sectional, low-resolution STEM-HAADF images of sample surface before and after treatment, respectively.

Computational details for STEM-EELS data

The simulations of O *K* edge XANES spectra were performed with the FDMNES code[1] and used the experimental orthorhombic $LaFeO_3$ structure of Selbach *et al.*[2] Although EELS and XANES are not strictly equivalent techniques, they probe the same electronic states. Therefore, a comparison between experimental and theoretical spectra across the two techniques provide invaluable insight and are commonly used to rationalize observed trends and fine structure features in oxides.[3] In FDMNES, the final excited state is obtained by solving a Schrödinger-like equation through the Greens formalism, within the limit of the muffin-tin approximation. The potentials and Fermi energy were determined self-consistently using a radii of 7 Å. Similar radii were used for the calculations of the spectra. Real Hedin-Lundquist potentials[4] were used to model the exchange-correlation. Dipoles, quadrupoles, core-hole and spin-orbit contributions were taken into account. A Hubbard correction of 4 eV has been applied to the localized valence orbitals of the Fe species.

In the case of oxygen interstitial, the atomic coordinates have been relaxed by density functional theory simulations (DFT) prior to calculating the XANES with FMNDES, while fixing the lattice parameters to their experimental values. The DFT calculations were performed with the VASP package[5] and used the PBEsol exchange-correlation functional.[6] The calculations of interstitial oxygen in orthorhombic $LaFeO_3$ used a 2×2×2 supercell of the experimental structure from Selbach *et al*. The cutoff energy for the plane wave basis set was fixed to 550 eV and a Monkhorst-Pack[7] *k*-points mesh of 2×2×2 for the sampling of the Brillouin zone was used. The total energy was converged to 10^{-5} eV/cell and the force components on the atoms were relaxed to below 10^{-4} eV/Å. Spin-polarization were used and the GGA+U method, as described by Dudarev,[8] was applied for the Fe atoms to correct the description of the Coulomb repulsion of the 3d electrons in standard GGA. The Hubbard parameter, *U*, describing the Coulomb interaction, was fixed to 5 eV, while the screened exchange energy, *J*, was fixed to 1 eV.

	Deformation	a (Å)	b (Å)	c (Å)	Fe—O—Fe (°) (in-plane)	Fe—O—Fe (°) (out-of-plane)	dFe—O (Å) (in-plane)	dFe—O (Å) (out-of-plane)
	Reference (Expt.)	5.554	5.566	7.853	154.81	157.37	1.975/2.053	2.002
Independent variation of lattice parameters	a expansion (5%)	5.832	5.566	7.853	155.30	156.30	2.033/2.093	2.006
	a contraction (5%)	5.276	5.566	7.853	154.31	158.46	1.919/2.014	1.999
	b expansion (5%)	5.544	5.844	7.853	155.27	157.39	2.012/2.111	2.002
	b contraction (5%)	5.544	5.288	7.853	154.32	157.40	1.994/1.938	2.002
	c expansion (5%)	5.544	5.566	8.346	153.56	158.72	1.978/2.056	2.123
	c contraction (5%)	5.554	5.566	7.460	155.78	156.21	2.049/1.972	1.906
Deformations based on LFO/SFO lattice mismatch	LFO (2a,2b)/STO (3a,3a)	5.858	5.858	7.853	155.79	156.17	2.078/2.159	2.006
	LFO (-2a,-2b)/STO (3a,3a)	5.263	5.263	7.853	153.70	158.53	1.947/1.875	1.998
	LFO (2b,1c)/STO (3a,2a)	5.554	5.858	7.810	155.42	157.23	2.015/2.115	1.992
	LFO (-2b,-1c)/STO (3a,2a)	5.554	5.263	7.896	154.17	157.52	1.990/1.935	2.013
Variation of octahedral tilt	No octahedral tilt	5.554	5.566	7.853	180.00	180.00	1.966/1.966	1.963
	Increase In-plane Oct. tilt	5.554	5.566	7.853	156.36	157.37	1.893/2.124	2.002
	Reduction In-plane Oct. tilt	5.554	5.566	7.853	151.25	157.37	1.954/2.105	2.002
Variation of lattice angle	Latt. Angle α (95°)	5.554	5.566	7.853	154.23/154.23	157.37	2.079/1.954	1.997
	Latt. Angle α (85°)	5.554	5.566	7.853	155.46/155.46	157.37	2.027/1.997	2.007
	Latt. Angle β (95°)	5.554	5.566	7.853	154.25/155.44	157.45	2.031/1.949	2.035
	Latt. Angle β (85°)	5.554	5.566	7.853	155.44/154.25	157.45	2.074/2.001	1.969
	Latt. Angle γ (95°)	5.554	5.566	7.853	156.01/153.45	157.11	2.136/1.893	2.003
	Latt. Angle γ (85°)	5.554	5.566	7.853	153.45/156.01	157.65	1.967/2.055	2.001

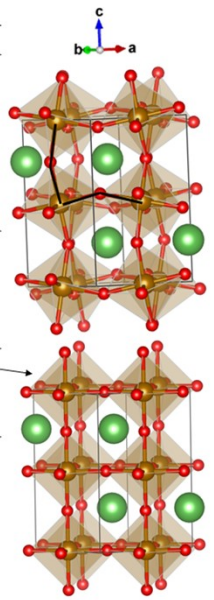

Table S5. List of the structural deformations investigated. Atoms represented by green, orange, and red balls are La, Fe, and O species respectively.

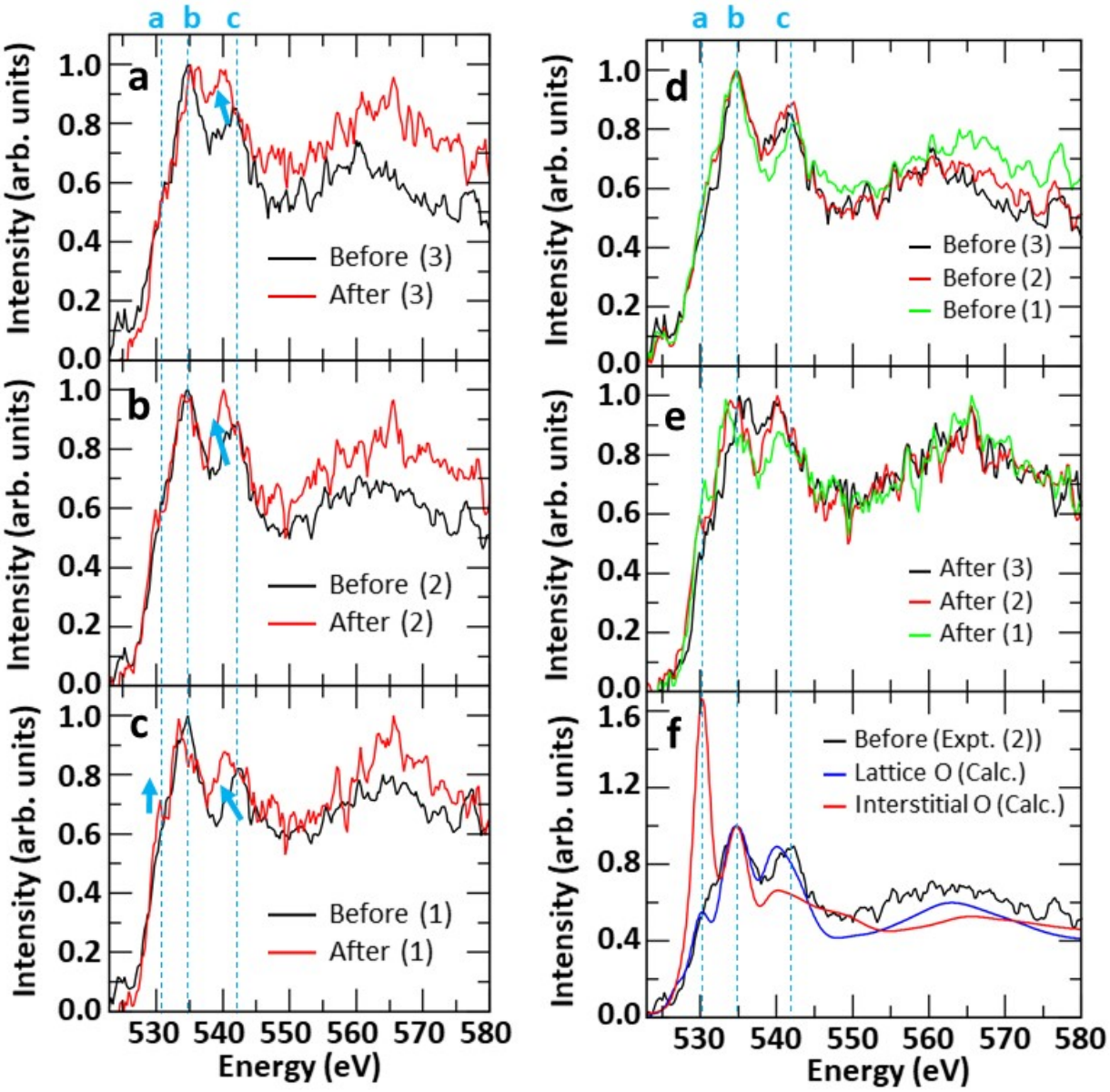

Figure S8. Comparison of experimental O *K* edge spectra before and after electrocatalysis for the different regions (1), (2), and (3) corresponding the film-substrate interface, middle, and film's surface respectively (a-e). (f) Comparison between experimental (2) and calculated spectra for lattice oxygen and interstitial oxygen.

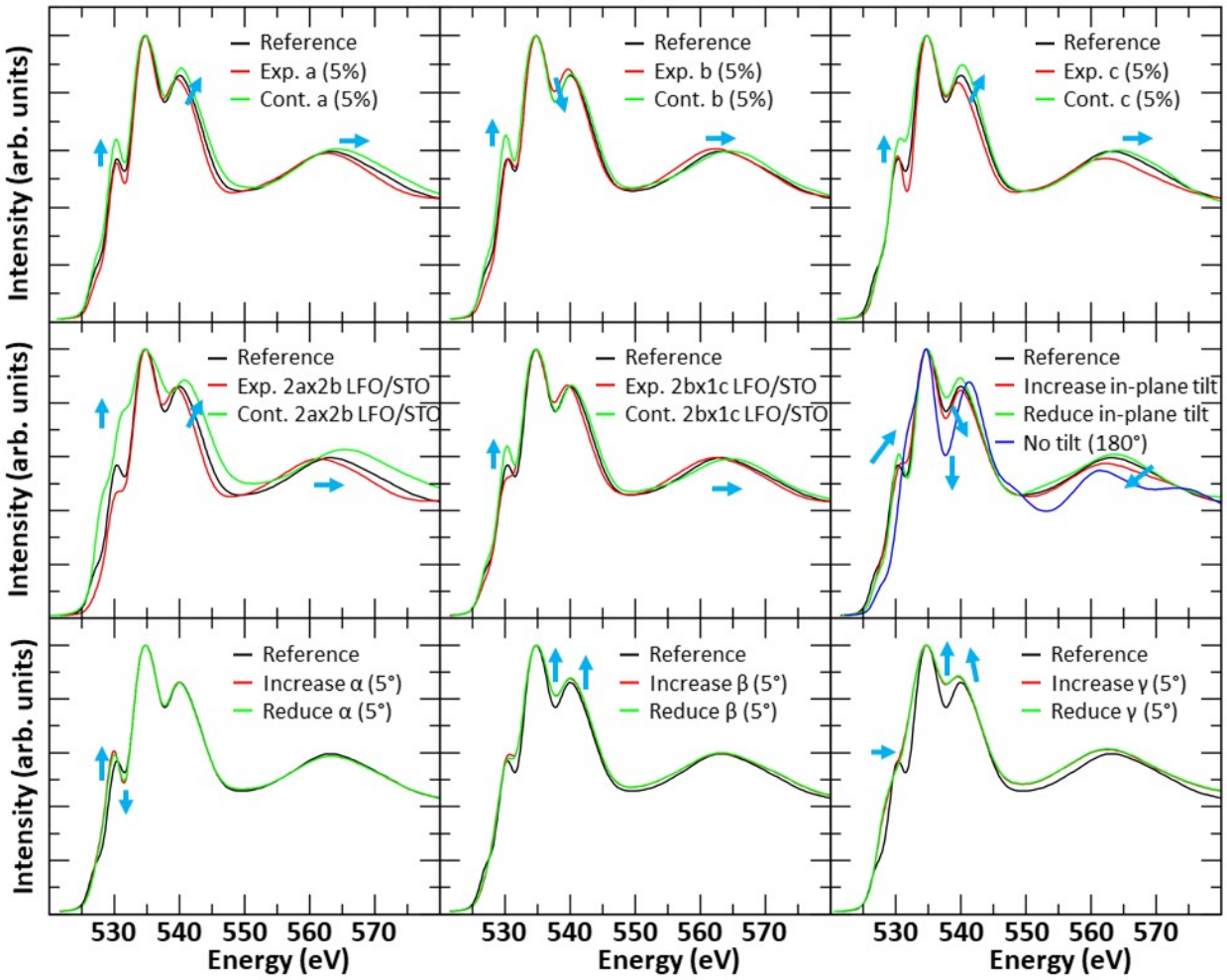

Figure S9. Comparison of the spectral changes as induced by various structural deformations listed in **Table S4**.

References

1. Bunău, O.; Joly, Y. Self-consistent aspects of x-ray absorption calculations. *Journal of Physics: Condensed Matter* **2009**, *21*, 345501.
2. Selbach, S.M.; Tolchard, J.R.; Fossdal, A.; Grande, T. Non-linear thermal evolution of the crystal structure and phase transitions of $LaFeO_3$ investigated by high temperature X-ray diffraction. *Journal of Solid State Chemistry* **2012**, *196*, 249-254.
3. Steven R. Spurgeon, Prasanna V. Balachandran, Despoina M. Kepaptsoglou, Anoop R. Damodaran, J. Karthik, Siamak Nejati, Lewys Jones, Haile Ambaye, Valeria Lauter, Quentin M. Ramasse, Kenneth K.S. Lau, Lane W. Martin, James M. Rondinelli, and Mitra L. Taheri. Polarization screening-induced magnetic phase gradients at complex oxide interfaces. Nature Communications 2015, 6, 6735.
4. Hedin, L.; Lundqvist, B.I. Explicit local exchange-correlation potentials *J. Phys. C: Solid State Phys.* **1971**, *4*, 2064.
5. Kresse, G.; Furthmuller, J. Efficient iterative schemes for ab initio total-energy calculations using a plane-wave basis set. *Phys. Rev. B* **1996***, 54*, 11169-11186.
6. Perdew, J.P.; Ruzsinszky, A.; Csonka, G.I.; Vydrov, O.A.; Scuseria, G.E.; Constantin, L.A.; Zhou, X.; Burke, K. Restoring the Density-Gradient Expansion for Exchange in Solids and Surfaces. *Physical Review Letters* **2008**, *100*, 136406.
7. Monkhorst, H.J.; Pack, J.D. Special points for Brillouin-zone integrations. *Physical Review B* **1976**, *13*, 5188-5192.
8. Dudarev, S.L.; Botton, G.A.; Savrasov, S.Y.; Szotek, Z.; Temmerman, W.M.; Sutton, A.P. Electronic structure and elastic properties of strongly correlated metal oxides from first principles: LSDA+U, SIC-LSDA and EELS study of UO_2 and NiO. *Phys. Status Solidi.* **1998**, *166*, 429-443.